Langmuir
Article
pubs.acs.org/Langmuir

A Unified Theory of Instabilities in Viscoelastic Thin Films: From Wetting to Confined Films, From Viscous to Elastic Films, and From Short to Long Waves

Jayati Sarkar[†] and Ashutosh Sharma*[,‡,§]

[†]*Department of Chemical Engineering, Indian Institute of Technology, Delhi 110016, India,*
[‡]*Department of Chemical Engineering, Indian Institute of Technology, Kanpur 208016, India, and*
[§]*School of Mechanical Engineering, Yeungnam University, Gyongsan 712-749, South Korea*

Received December 29, 2009. Revised Manuscript Received February 17, 2010

A general unified theory of field (van der Waals, electric, etc.)-induced surface instabilities in thin viscoelastic films that accounts for a destabilizing field and stabilizing effects of elastic strain and surface energy is presented. The present theory seamlessly covers the instability and its different regimes in films ranging from elastic to viscous, from adhesive (confined) to wetting (free surface), and from short- to long-wave instabilities. The critical conditions for the onset of instability are found to be strongly dependent on elastic properties such as the shear modulus of the film, but the dominant wavelength is strikingly independent of the film rheology. Different regimes based on a nondimensional parameter ($\gamma/\mu h$) are uncovered, where γ is the surface energy, μ is the elastic shear modulus, and h is the film thickness. A short-wave, elasticlike response with wavelength $\lambda \approx 2.96h$ is obtained for $\gamma/\mu h < 0.1$, whereas long waves that depend nonlinearly on the field strength and surface energy are obtained for $\gamma/\mu h > 1$. Owing to their small critical thickness, wetting films destabilized by intermolecular forces always display long-wave instability regardless of their viscoelasticity. Furthermore, our numerical simulations based on energy minimization for unstable wetting elastic films show the formation of islands for ultrathin films and a morphological phase transition to holes embedded in the film for relatively thicker films. Unlike viscous films, however, unstable elastic films do not display a unique dominant wavelength but a bimodal distribution of wavelengths.

Introduction

Mesomechanics of thin viscous[1−34] and elastic films[35−56] has generated widespread interest because of their scientific and technological contents ranging from wetting−dewetting and adhesion−debonding to opto-electronic coatings and structures. Mesomechanical considerations are important both in producing a stable thin film and in controlled destruction to engineer desired

*Corresponding author. E-mail: ashutos@iitk.ac.in.

(1) Ruckenstein, E.; Jain, R. K. *J. Chem. Soc., Faraday Trans. 2* **1974**, *70*, 132.
(2) Reiter, G. *Langmuir* **1993**, *9*, 1344.
(3) Sharma, A.; Jameel, A. T. *J. Colloid Interface Sci.* **1993**, *161*, 190.
(4) Sharma, A. *Langmuir* **1993**, *9*, 861.
(5) Sharma, A.; Reiter, G. *J. Colloid Interface Sci.* **1996**, *178*, 383.
(6) Sharma, A.; Khanna, R. *Phys. Rev. Lett.* **1998**, *81*, 3463.
(7) Xie, R.; Karim, A.; Douglas, J. F.; Han, C. C.; Weiss, R. A. *Phys. Rev. Lett.* **1998**, *81*, 1251.
(8) Reiter, G.; Khanna, R.; Sharma, A. *Phys. Rev. Lett.* **2000**, *85*, 1432.
(9) Oron, A. *Phys. Rev. Lett.* **2000**, *85*, 2108.
(10) Konnur, R.; Kargupta, K.; Sharma, A. *Phys. Rev. Lett.* **2000**, *84*, 931.
(11) Kargupta, K.; Konnur, R.; Sharma, A. *Langmuir* **2000**, *16*, 10243.
(12) Seeman, S.; Herminghaus, S.; Jacobs, K. *Phys. Rev. Lett.* **2001**, *86*, 5534.
(13) Besterhorn, M.; Neuffer, K. *Phys. Rev. Lett.* **2001**, *87*, 046101.
(14) Zope, M.; Kargupta, K.; Sharma, A. *J. Chem. Phys.* **2001**, *114*, 7211.
(15) Deshpande, P.; Sun, X.; Chou, S. Y. *Appl. Phys. Lett.* **2001**, *79*, 1688.
(16) Kargupta, K.; Sharma, A. *J. Colloid Interface Sci.* **2002**, *245*, 99.
(17) Wensink, K. D. F.; Jerome, B. *Langmuir* **2002**, *18*, 413.
(18) Sharma, A.; Mittal, J. *Phys. Rev. Lett.* **2002**, *89*, 186101.
(19) Sharma, A.; Mittal, J.; Verma, R. *Langmuir* **2002**, *18*, 10213.
(20) Sehgal, A.; Ferreiro, V.; Douglas, J. F.; Amis, E. J.; Karim, A. *Langmuir* **2002**, *18*, 7041.
(21) Bestehorn, M.; Pototsky, A.; Thiele, U. *Eur. Phys. J. B* **2002**, *33*, 457.
(22) Sharma, A. *Eur. Phys. J. E* **2003**, *12*, 397–408.
(23) Kao, J. C. T.; Golovin, A. A.; Davis, S. H. *J. Colloid Interface Sci.* **2006**, *303*, 532.
(24) Verma, R.; Sharma, A.; Benarjee, I.; Kargupta, K. *J. Colloid Interface Sci.* **2006**, *296*, 220–232.
(25) Suman, B.; Kumar, S. *J. Colloid Interface Sci.* **2006**, *304*, 208–213.
(26) Lenz, R. D.; Kumar, S. *J. Fluid Mech.* **2007**, *571*, 33–57.
(27) Mukherjee, R.; Bandyopadhyay, D.; Sharma, A. *Soft Matter* **2008**, *4*, 2086–2097.
(28) Craster, R. V.; Matar, O. K. *Rev. Mod. Phys.* **2009**, *81*, 1131–1198.
(29) Schäffer, E.; Thurn-Albrecht, T.; Russel, T. P.; Steiner, U. *Nature* **2000**, *403*, 874–877.
(30) Morariu, M. D.; Voicu, N. E.; Schäffer, E.; Lin, Z.; Russell, T. P.; Steiner, U. *Nat. Mater.* **2003**, *2*, 48.
(31) Harkema, S.; Steiner, U. *Adv. Funct. Mater.* **2005**, *15*, 2016.
(32) Verma, R.; Sharma, A.; Kargupta, K.; Bhaumik, J. *Langmuir* **2005**, *21*, 3710–3721.
(33) Wu, N.; Pease, L. F., III; Russel, W. B. *Adv. Funct. Mater.* **2006**, *16*, 1992.
(34) Voicu, N. E.; Harkema, S.; Steiner, U. *Adv. Funct. Mater.* **2006**, *16*, 926.
(35) Kumar, S. *Langmuir* **2003**, *19*, 2473–2478.
(36) Reiter, G. *Phys. Rev. Lett.* **2001**, *87*, 186101.
(37) Ghatak, A.; Chaudhury, M. K.; Shenoy, V.; Sharma, A. *Phys. Rev. Lett.* **2000**, *85*, 4329–4332.
(38) Shull, K. R.; Flanigan, C. M.; Crosby, A. J. *Phys. Rev. Lett.* **2000**, *84*, 3057–3060.
(39) Mönch, W.; Herminghaus, S. *Europhys. Lett.* **2001**, *53*, 525–531.
(40) Shenoy, V.; Sharma, A. *Phys. Rev. Lett.* **2001**, *86*, 119–122.
(41) Shenoy, V.; Sharma, A. *J. Mech. Phys. Solids* **2002**, *50*, 1155–1173.
(42) Ru, C. Q. *J. Appl. Mech.* **2002**, *69*, 97–103.
(43) Ghatak, A.; Chaudhury, M. K. *Langmuir* **2003**, *19*, 2621–2631.
(44) Webber, R. E.; Shull, K. R.; Roos, A.; Creton, C. *Phys. Rev. E* **2003**, *68*, 021805 (11).
(45) Sarkar, J.; Shenoy, V.; Sharma, A. *Phys. Rev. E* **2003**, *67*, 031607.
(46) Sarkar, J.; Shenoy, V.; Sharma, A. *Phys. Rev. Lett.* **2004**, *93*, 018302.
(47) Sarkar, J.; Sharma, A.; Shenoy, V. *Langmuir* **2005**, *21*, 1457.
(48) Gonuguntala, M.; Sharma, A.; Sarkar, J.; Subramanian, S. A.; Ghosh, M.; Shenoy, V. *Phys. Rev. Lett.* **2006**, *97*, 018303.
(49) Gonuguntala, M.; Sharma, A.; Mukharjee, R.; Subramanian, S. A. *Langmuir* **2006**, *22*, 7066–7071.
(50) Chung, J.-Y.; Kim, K.; Chaudhury, M. K.; Sarkar, J.; Sharma, A. *Eur. Phys. J. E* **2006**, *20*, 47–53.
(51) Tomar, G.; Sharma, A.; Shenoy, V.; Biswas, G. *Phys. Rev. E* **2007**, *76*, 011607.
(52) Sharma, A.; Gonuguntla, M.; Mukherjee, R.; Subramanian, S. A.; Pangule, R. K. *J. Nanosci. Nanotechnol.* **2007**, *7*, 1744–1752.
(53) Sarkar, J.; Sharma, A.; Shenoy, V. *J. Adhes.* **2005**, *81*, 271–295.
(54) Arun, N.; Sharma, A.; Shenoy, V.; Narayan, K. S. *Adv. Mater.* **2006**, *18*, 660–663.
(55) Arun, N.; Sarkar, J.; Sharma, A.; Shenoy, V; Narayan, K. S. *J. Adhes.* **2007**, *83*, 513–534.

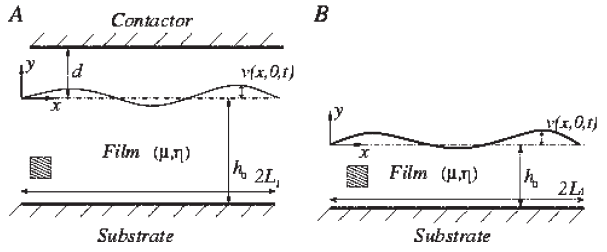

Figure 1. (A) Incompressible viscoelastic film with mean thickness h_0 bonded rigidly to a substrate and subjected to attractive interactions from a contactor plate held a distance d from the undeformed film surface. This is the case for an adhesive film. (B) Wetting, incompressible viscoelastic film with parameters h_0, μ, and η resting on a substrate and subjected to excess attractive interactions arising from the small thickness of the film.

mesopatterns. We develop here a unified theory of stability for viscoelastic films, for which we will use the following nomenclature to refer to different thin film situations of experimental interest. A "dewetting film or wetting film or free film" will refer to a viscoelastic film with a free surface that is supported on a rigid solid substrate without slip. An "adhesive film or confined film" refers to the situation of a viscoelastic film confined between two solid surfaces, bonded without any slip to its substrate and confined by a field (van der Waals or electric) originating from another surface in its vicinity. Figure 1 displays a schematic of these two situations. The major difference between the two systems is that in an unstable (de)wetting film the destabilizing intersurface interactions grow stronger with a reduction in the film thickness but so do stabilizing factors such as the surface tension and elasticity. In a confined film, the film thickness usually plays a minor role in determining the destabilizing force, which becomes stronger with increasing external field intensity (e.g., by the increased proximity of the film surface to the confining surface or contactor).

The mesomechanics of thin films has evolved basically along two distinct routes—a purely viscous film supported on a solid substrate (a special case of the free film, the so-called wetting film) and a soft, purely elastic film sandwiched between two substrates (a special case of the adhesive film). Ultrathin (< 100 nm) liquid films (usually polymeric melts) dewet spontaneously by a long wave-instability (wavelength ≫ thickness), the wavelength and thickness scaling of which seem to be in agreement with predictions of a purely viscous model, notwithstanding the elasticity polymeric melts displayed.[3−14,16−34] Furthermore, the wavelength of instability in this so-called spinodal dewetting depends strongly on the intermolecular potential and the surface tension. Elastic thin polystyrene films (PS)[36] as well as ultrathin (< 3 nm)[57,58] solid free films have also been observed to undergo dewetting and roughening by long-wave instability, as do weakly elastic free liquid-crystal films.[59] Some PS films prepared by varying molecular weight[60,61] exhibit a critical thickness below which instability is manifested. Soft viscoelastic free films may thus also display a similar critical thickness (or critical shear modulus), which is in contrast to purely viscous films that are theoretically shown to be unconditionally unstable for a monotonically decaying disjoining pressure (such as the long-range van der Waals attraction). The observations regarding the roughening of elastic free films are theoretically not well understood. This observation is even more surprising considering that micrometer-sized or even thicker, purely elastic adhesive films spontaneously develop a short-wave instability (wavelength ∼ thickness) during the process of adhesion[37−53] or the imposition of an electric field.[54−56] The initial formation of interfacial cavities manifests as microscopic bubbles or bridges between the substrates as they are pulled apart to debond. Even more surprising is the fact that the wavelength in this case is independent of the surface tension and the intermolecular potential (between the contacting substrate and the film surface) and is thus independent of the surface energies of the contactor and the film![37−56]

As a brief summary, both the existing observations and theories suggest that ultrathin free films dewet by a long-wave instability and their wavelength depends exclusively on the surface tension force and the interactions between the film and the substrate, whereas thicker, purely elastic adhesive films debond by a short-wave instability that is completely independent of the surface tension and details of the intersurface interactions! The purpose of this article is to develop a unified mesomechanical understanding of these two apparently unrelated phenomena and establish conditions under which one or the other is manifested. There are some recent theoretical studies on electric-field-induced instabilities in liquidlike viscoelastic films[62,63] and solid films.[64] However, a general theory of viscoelastic thin films that seamlessly encompasses all of the limits in the presence of a generic force field has never been studied. In this article, we carry out a linear stability analysis of a linear viscoelastic thin film subjected to an arbitrary force field and present some simulations for purely elastic films because simulations for purely viscous ultrathin films have already been extensively reported in the literature.[3,5,6,9−11,13,14,16,18,19,21−28,32] Such an approach will allow a unified understanding of thin film instabilities in a variety of contexts, including different regimes of instability and the transitions among them as well as the roles of film rheology, thickness, surface energy, and the destabilizing force field on the length scale and dynamics of instability in both free and adhesive films.

Theory

Schematic diagrams in Figure 1A,B show a viscoelastic film of thickness h_0 undergoing adhesion and dewetting, respectively. On the approach of a contactor (Figure 1A), the adhesive film deforms under the influence of the intermolecular forces.[37−53] In contrast, a thin film can dewet because of the excess intermolecular interactions with its substrate (Figure 1B).[1−34] The dynamics of thin films (Figure 1) can be described by the governing equations of motion, neglecting gravitational and inertial forces,

$$\vec{\nabla}\cdot\underline{\sigma} = 0 \tag{1}$$

where $\underline{\sigma}$ is the stress tensor. As is customary in thin film dynamics, the inertial effects are neglected[1−19] because the films considered are thin (< 1000 μm) in the case of a confined film and ultrathin (< 100 nm) in the case of a wetting film destabilized by van der

(56) Sarkar, J.; Sharma, A.; Shenoy, V. *Phys. Rev. E* **2008**, *77*, 031604.
(57) Buschbaum, P. M. *Eur. Phys. J. E* **2003**, *12*, 443.
(58) Bollinne, C.; Cuenot, S.; Nysten, B.; Jonas, A. M. *Eur. Phys. J. E* **2003**, *12*, 389–396.
(59) Herminghaus, S.; Jacobs, K.; Mecke, K.; Bischof, J.; Fery, A.; Ibn-Elhaj, M.; Schlagowski, S. *Science* **1998**, *282*, 916–919.
(60) Rehse, N.; Wang, C.; Hund, M.; Geoghegan, M.; Magerle, R.; Krausch, G. *Eur. Phys. J. E* **2001**, *4*, 69.
(61) Aubouy, M. *Phys. Rev. E* **1997**, *56*, 3370.
(62) Tomar, G.; Shankar, V.; Shukla, A.; Sharma, A.; Biswas, G. *Eur. Phys. J. E* **2006**, *20*, 185–200.
(63) Tomar, G.; Shankar, V.; Sharma, A.; Biswas, G. *J. Non-Newtonian Fluid Mech.* **2007**, *43*, 120–130.
(64) Arun, N.; Sharma, A.; Partho, S.; Pattader, G.; Banerjee, I.; Dixit, H. M.; Narayan, K. S. *Phys. Rev. Lett.* **2009**, *102*, 254502.

Waals interaction. Furthermore, in the case of elastic films, the timescale, when it is of experimental interest, is much longer than the time for the propagation of elastic waves through the film.[37−56]

As shown in Figure 1, the displacement and velocity vectors of the film are $\mathbf{u}$ and $\dot{\mathbf{u}}$, respectively, which vary with spatial coordinates x and y and with time t. The superscript denotes the time derivative. For an incompressible film,

$$\vec{\nabla}\cdot\mathbf{u} = 0 \text{ and } \vec{\nabla}\cdot\dot{\mathbf{u}} = 0 \tag{2}$$

The constitutive relation is chosen to be a zero-frequency linear viscoelastic model,

$$\underline{\sigma} = p\mathbf{I} + \mu(\vec{\nabla}\mathbf{u} + \vec{\nabla}\mathbf{u}^{\mathrm{T}}) + \eta(\vec{\nabla}\dot{\mathbf{u}} + \vec{\nabla}\dot{\mathbf{u}}^{\mathrm{T}}) \tag{3}$$

where p is the pressure across the film. The parameters μ and η are the shear modulus and the viscosity of the film, respectively.

By substituting eqs 2 and 3 into eq 1, the equation of motion is modified to

$$\vec{\nabla}p + \mu\nabla^2\mathbf{u} + \eta\nabla^2\dot{\mathbf{u}} = 0 \tag{4}$$

We assume that both of the films (adhesive and dewetting) are bonded rigidly to the underlying substrate. No-slip and impermeability boundary conditions are employed at the film−substrate interface at the coordinate $y = -h_0$. Thus,

$$\mathbf{u}(x, -h_0, t) = \mathbf{0} \tag{5}$$

and

$$\dot{\mathbf{u}}(x, -h_0, t) = \mathbf{0} \tag{6}$$

The free surface of the film (at the coordinate $y = 0$) is assumed to be shear-free:

$$\sigma_{yx}(x, 0, t) = 0 \tag{7}$$

The normal stress balance at the free surface yields

$$\sigma_{yy}(x, 0, t) = \gamma v_{xx}(x, 0, t) - \phi(x, 0, t) \tag{8}$$

Here, the first term on the right-hand side represents the surface tension force where γ is the surface energy, with v being the y component of displacement. The normal displacement at the free surface is thus represented by the quantity $v(x, 0, t)$. The above formalism and the linear stability analysis below are valid for any arbitrary interaction force $\phi = \partial\Delta G/\partial v$, which is related to the interaction energy per unit area, $\Delta G(\xi)$. Here, ξ is an effective intersurface distance between the surfaces undergoing an attractive force. For an adhesive film, $\xi = d_0 - v(x, 0, t)$, which is the gap distance between the contactor and the film surface. For a dewetting film, $\xi = h_0 + v(x, 0, t)$, which is the film thickness. For illustration, we chose the van der Waals force $\phi = \partial\Delta G/\partial v$, where $\Delta G = -A/12\pi\xi^2$ is the van der Waals energy per unit area and A ($\sim 10^{-20}$ J) is the Hamaker constant. Other forms of the potential (e.g., electric field potential) can also be readily used in the derivations presented here.

It may be noted that the van der Waals potential chosen here neglects the effects of surface curvature, which is a good approximation for long-wave instabilities.[1−28] Even though we do not assume long waves, a major conclusion that we will show on the basis of the analysis below is that the instabilities in a "free" or wetting van der Waals film are indeed always long-wave, regardless of the film's viscoelasticity, including instabilities in purely elastic films. For adhesive or confined films that are nearly elastic, instabilities can be short-wave but their length scale becomes independent of the form of the destabilizing potential![37−56] In fact, all that is required is a critical magnitude of the attractive destabilizing force; the precise form of the potential is not important.[37−56]

Linear Stability Analysis

To perform linear stability analysis, the interaction energy is expanded in a Taylor series about the reference state of the undeformed film. By retaining terms up to second order, the interaction energy has the form

$$\Delta G(v(x, 0, t)) = \Delta G_0 + Fv(x, 0, t) + \frac{Yv(x, 0, t)^2}{2} \tag{9}$$

For an adhesive film, the VDW interactions have the following form

$$\Delta G_0 = \Delta G(0) = -\frac{A}{12\pi {d_0}^2},\ F = -\Delta G'(0) = -\frac{A}{6\pi {d_0}^3},$$
$$Y = \Delta G''(0) = -\frac{A}{2\pi {d_0}^4} \tag{10}$$

and for a dewetting film, they are

$$\Delta G_0 = \Delta G(0) = -\frac{A}{12\pi {h_0}^2},\ F = \Delta G'(0) = \frac{A}{6\pi {h_0}^3},$$
$$Y = \Delta G''(0) = -\frac{A}{2\pi {h_0}^4} \tag{11}$$

Thus, the interaction force acting at the surface of the film is of the form

$$\phi = F + Yv(x, 0, t) \tag{12}$$

The homogeneous solution of the viscoelastic differential equation (eq 4) along with the boundary conditions (eqs 5−8) is that of zero displacement, and the corresponding pressure field is given by

$$p(x, y, t) = -F \tag{13}$$

From eqs 10 and 11, it is evident that for an adhesive film $p(x, y, t) = A/6\pi {d_0}^3$ and for a dewetting film $p(x, y, t) = -A/6\pi {h_0}^3$. Therefore, during adhesion, the pressure across the film is tensile, whereas for a dewetting film, the pressure is compressive in nature, helping in both cases to engender surface instabilities.

To obtain the inhomogeneous solution, the homogeneous solution is superimposed on a perturbation of the form

$$\mathbf{u}(x, y, t) = \mathrm{e}^{\mathrm{i}kx}\mathbf{u}(y)\mathrm{e}^{\omega t} \tag{14}$$

$$p(x, y, t) = \mathrm{e}^{\mathrm{i}kx}p(y)\mathrm{e}^{\omega t} \tag{15}$$

Here, ω is the linear growth rate and k is the wavenumber of the pertubation. A positive (negative) value of ω indicates instability (stability).

Linearization of the equation of motion (eq 4) along with the boundary conditions (eqs 5−8) using the normal linear modes (eqs 14 and 15) leads to the following dispersion relation

$$\omega = \frac{-Y - \gamma k^2}{2kS(kh)\eta} - \frac{\mu}{\eta} \tag{16}$$

where $S(q) = \frac{(1+\mathrm{e}^{2q})^2 + 4\mathrm{e}^{2q}q^2}{(-1+\mathrm{e}^{4q}) - 4\mathrm{e}^{2q}q}$ and $q = kh$.

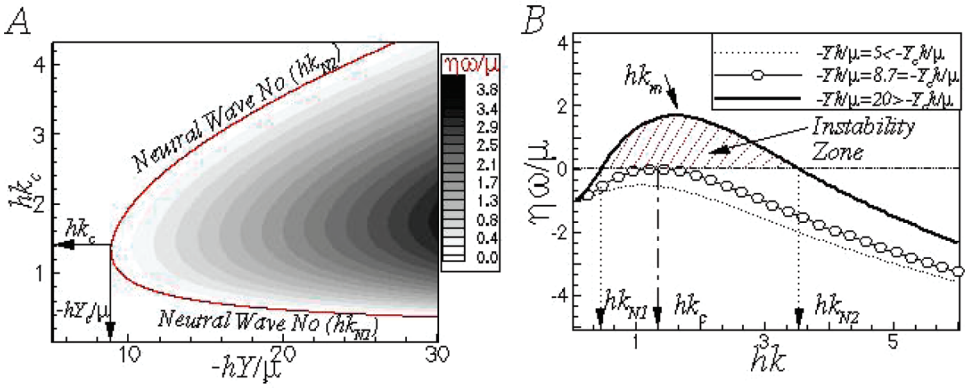

Figure 2. (A) Bifurcation diagram showing regions of instability both for adhesive and wetting films for $\gamma/\mu h = 1$. The inception of instability occurs when the interaction stiffness reaches a critical value $-hY_c/\mu$. (B) Cross-sectional view of the bifurcation diagram in A for values of the interaction stiffness less than, equal to, and greater than the critical value. The instability growth rate is positive only when $-hY/\mu > -hY_c/\mu$.

Asymptotic Cases. The two simpler limiting cases of the general dispersion relation are discussed first to motivate a fuller understanding of eq 16.

(*i*) *Viscous Films* ($\mu \rightarrow 0$). The linear dispersion relation for the dewetting/free[1−23,25−28] and confined/adhesive viscous films[24] can be obtained from the dispersion relation (eq 16) by setting the elastic shear modulus equal to zero, which gives

$$\omega = \frac{-Y - \gamma k^2}{2kS(kh)\eta} \tag{17}$$

This is a well-known result[3−11,13,14,16−19,21−28,32] from which it is easily verified that a viscous film is unconditionally unstable with respect to a band of long waves for attractive interactions ($Y < 0$), regardless of their strength. An important point to note is that there is no critical parameter to be tuned for the onset of instability in a viscous film except for the critical wavelength itself, which can become important only if the lateral dimension of the film becomes comparable to the wavelength—on the order of micrometers. Thus, in experiments with viscous liquidlike films, one observes only the dominant or the fastest growing wave if it grows within the laboratory timescale. Furthermore, the dominant long wavelength of instability ($d\omega/dk = 0$) depends nonlinearly on the strength of the destabilizing force, surface tension, and film thickness but is independent of viscosity.

(*ii*) *Elastic Films* ($\eta \rightarrow 0$). In cases of both dewetting and adhesive elastic films, the dispersion relation (eq 16) yields the critical condition for the onset of the instability realized by setting the neutral stability condition ($\omega = 0$) and the viscosity equal to zero,[41,48]

$$2qS(q) = -\left(\frac{\gamma}{\mu h}\right)q^2 - \frac{hY}{\mu} \tag{18}$$

Unlike the case of a viscous film, the onset of instability in a purely elastic film requires a finite critical destabilizing force.[37,39−43,45−56]

A further simplification of the above result is obtained for thick micrometer-sized films where the surface tension force becomes weak,[40−42,45−47,51,53−56] and eq 18 can be further reduced to

$$2qS(q) = -\frac{hY}{\mu} \tag{19}$$

The critical force required to cause instability in elastic adhesive films corresponds to the minimum Y for which eq 19 yields positive finite solutions of q.[40−42,45−47,51,53−56] The minimum of $-hY/\mu$ is 6.22, and the corresponding critical wavelength is obtained as $\lambda/h = 2\pi/q = 2.96$.[37−43,45−56] The length scale in this short-wave regime is on the order of the thickness of the film and is independent of the destabilizing force, surface energy, and rheology. It may be remembered, however, that this result corresponds to the critical conditions at the onset of instability in a purely elastic, relatively thick film. Physically, this critical wavelength is observed in the experiments where one of the bifurcation parameters (electric field strength, film thickness, distance to the contactor, and elastic modulus) is varied until the instability is manifested for the first time.[39,48−50,52,54,55] In the adhesion−debonding experiments with elastic films, the critical wavelength continues to manifest itself even in the debonding phase as the surfaces are pulled apart because of the adhesive pinning of the critical structures to the contacting or retracting surface.[46,47,53] However, if an experiment is conducted such that the initial state is already deep within the unstable territory, then it is the dominant wave rather than the critical wave that becomes important. This can be realized, for example, by ramping up the voltage beyond the critical voltage at time $t = 0$. However, as discussed later, this issue becomes relevant only for a viscoelastic solidlike film where the dynamics is controlled by its viscosity. A purely elastic film has instantaneous dynamics when solid inertia is neglected.

In view of the above discussion, we present results for the behavior of both critical and dominant wavelengths.

The general dispersion relation can be recast in terms of nondimensional parameters $\eta\omega/\mu$, $-hY/\mu$, hk, and $\gamma/\mu h$,

$$\frac{\eta\omega}{\mu} = \frac{-\frac{hY}{\mu} - \left(\frac{\gamma}{\mu h}\right)q^2}{2qS(q)} - 1 \tag{20}$$

Parameters $\eta\omega/\mu$ and hk are the nondimensional growth rate and wavenumber, respectively. The other nondimensional quantities represent the ratio of the different forces operative in the films. Parameter $-hY/\mu$ is the ratio of the destabilizing interaction stiffness ($-Y$) and the elastic stiffness of the film (μ/h). This ratio is a measure of the effective destabilizing forces vis-à-vis the stabilizing elastic force. The quantity $\gamma/\mu h$ is the ratio of two stabilizing mechanisms—surface tension and the elastic force.

Results and Discussion

Linear Stability Analysis for Adhesive and Dewetting Viscoelastic Films. Figure 2A is the bifurcation diagram demarcating the regions of stability ($\eta\omega/\mu < 0$) and instability ($\eta\omega/\mu \geq 0$)

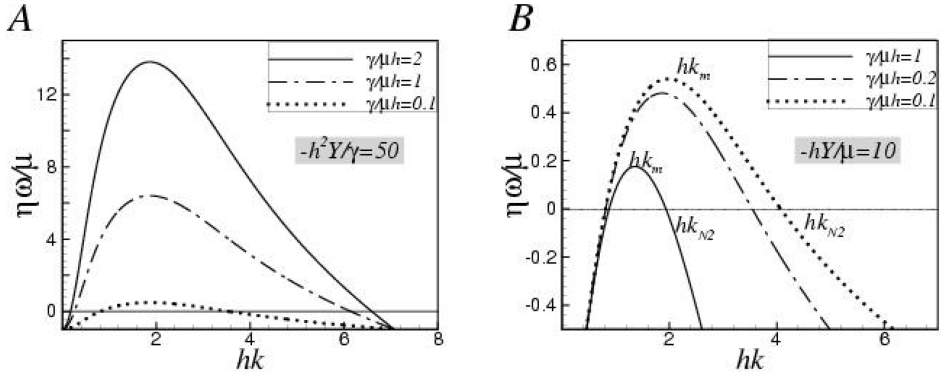

Figure 3. (A) Increasing elasticity (μ) (marked by lower values of $\gamma/\mu h$) shrinks the instability zone. (B) Increasing surface tension (γ) (marked by higher values of $\gamma/\mu h$) also shrinks the instability zone and shifts the neutral and dominant wavenumbers toward the long-wave limit.

(marked as the gray-scaled zone) in a typical viscoelastic film. Thus, neutral wavenumber $\eta\omega/\mu = 0$ is the boundary of the instability domain. In this Figure, parameter $\gamma/\mu h$ (= 1) is kept constant. The critical condition for the onset of instability is marked by the critical growth rate ($\eta\omega_c/\mu = 0$), critical interaction stiffness ($-hY_c/\mu$), and critical wavenumber hk_c. It is denoted by the point where two branches of the critical wavenumber emerge and continue on in the unstable region. If the interaction stiffness is greater than $-hY_c/\mu$, then there is a region bounded by two neutral or critical wavenumbers within which the growth rate is positive. A cross-sectional view of Figure 2A for three different values of the interaction stiffness is shown in Figure 2B. It indicates that for interaction stiffness lower than $-hY_c/\mu$ (namely, for wetting films with thickness greater than a critical value and for adhesive film with the contactor−film separation distance higher than the critical distance) the growth rate remains negative for all wavenumbers and the system is stable. However, for interaction stiffness greater than $-hY_c/\mu$, the growth rate is positive for a range of wavenumbers lying between hk_{N1} and hk_{N2}. Within this range of neutral wave numbers there is a dominant wavenumber, hk_m, where the growth coefficient is at its maximum ($\eta\omega/\mu = \eta\omega_m/\mu$). The critical condition thus essentially sees the merging of the two neutral wavenumbers and the dominant wavenumber to a single value of hk_c.

Figure 3 shows the influence of elasticity and surface tension on the instability characteristics. Figure 3A shows that for a constant value of $-h^2Y/\gamma$ (exceeding the critical value), the growth coefficient decreases and the range of unstable wavenumbers shrinks with a decrease in $\gamma/\mu h$. Similarly, for a fixed value of the interaction stiffness ($-hY/\mu$), as the nondimensional surface tension ($\gamma/\mu h$) increases, the growth coefficient decreases and the dominant wavenumber shifts to longer wavelengths (Figure 3B). Furthermore, the neutral wavenumber hk_{N2} also decreases.

To assess the ease of initiating the instability in films with different physical properties, the critical interaction stiffness ($-hY_c/\mu$) is plotted with $\gamma/\mu h$ as shown by the solid line in Figure 4. It is evident that $-hY_c/\mu = 6.22$ for $\gamma/\mu h < 10^{-2}$, which is indeed the asymptotic limit for elastic adhesive films.[40−42,45−47,51,53−56] In addition, Figure 4 shows that the critical nondimensional force $-hY_c/\mu$ increases monotonically with $\gamma/\mu h$. The Figure indicates that films with higher surface energy require a higher energy penalty for deformations of the elastic film and the films undergoing adhesion require a smaller contactor−film separation distance in order to acquire a higher destabilizing interaction energy. For dewetting films, the critical film thickness below which instability is possible decreases with increases in the surface tension force. To show the effects of the shear modulus clearly,

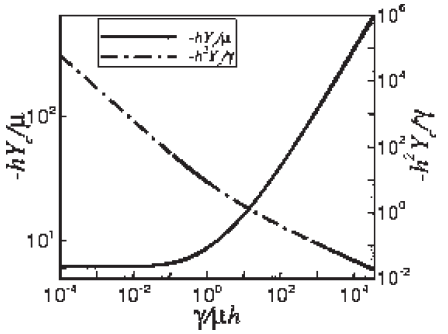

Figure 4. Critical interaction stiffness $-hY_c/\mu$ is an increasing function of $\gamma/\mu h$, indicating that the surface penalty required to overcome the interaction energy is higher for films with higher surface tension effects. Nondimension parameter $-h^2Y_c/\gamma$ decreases with $\gamma/\mu h$, showing that films with smaller elasticity effects (low values of shear modulus μ) are unconditionally unstable.

a nondimensional parameter $-h^2Y_c/\gamma$ is obtained from the ratio of $-hY_c/\mu$ to $\gamma/\mu h$. The broken line in Figure 4 shows that $-h^2Y_c/\gamma$ decreases monotonically with increasing $\gamma/\mu h$. The Figure indicates that for a lower shear modulus, namely, for more liquidlike films, the interaction energy required to bring about the inhomogeneity is negligibly small and thus for viscous films ($\mu \to 0$) the films indeed become unconditionally unstable. However, dewetting films even with a small elasticity may require a considerable amount of interaction force to initiate the instability. A quick calculation proves that a viscoelastic film would have to be very soft ($\mu \approx 1000$ Pa or less) for the van der Waals force to initiate instability in a wetting film of physically realizable and meaningful thickness (> 1 nm).

Figure 5 shows the variation of the critical wavenumber (hk_c) with $\gamma/\mu h$. The curve supplies the following set of interesting information: (i) For dewetting films, the instability is always long-wave regardless of its viscoelasticity because h has to be very low so that the van der Waals force is strong enough to initiate the instability and thus $\gamma/\mu h$ has to be high (low hk_c). (ii) For an adhesive film, the instability can be either long-wave (high $\gamma/\mu h$) or short-wave (low $\gamma/\mu h$). It is evident that for low values of $\gamma/\mu h$ ($< 10^{-2}$), $hk_c \approx 2.12$ becomes independent of $\gamma/\mu h$ and the critical wavelength ($\lambda_c = 2\pi/k_c$) approaches its elastic limit of $2.96h$.[37−56] In contrast, for higher values of $\gamma/\mu h$ (high γ or low μ), the critical wavelength increases considerably. In between the two distinct short- and long-wavelength regimes, there is a transition zone where $\gamma/\mu h$ is between 10^{-1} and 1.

As shown elsewhere,[41,48] for adhesive films of thickness $h > 1\ \mu$m, the surface tension forces ($\gamma/\mu h \ll 1$) are negligible and the

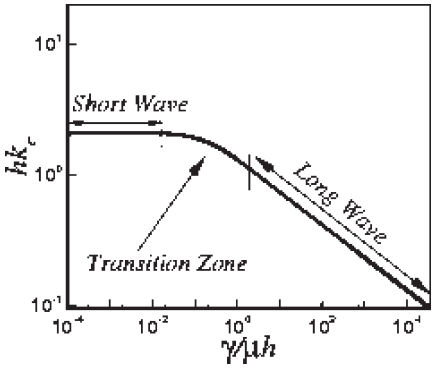

Figure 5. Critical wavenumber as a function of $\gamma/\mu h$. For $\gamma/\mu h < 10^{-2}$, hk_c is independent of surface tension effects and is constant at 2.12. The initiation of instability in this regime occurs in the short-wave regime. With increases in $\gamma/\mu h$, the initiation of instability occurs in the long-wave regime.

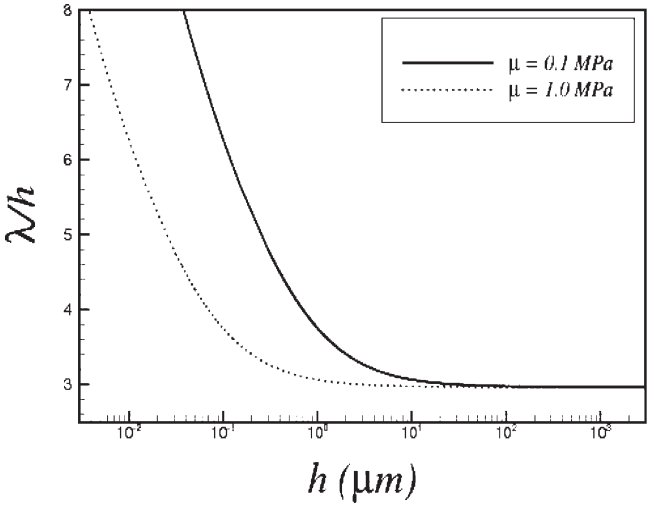

Figure 6. Transition of coefficient λ/h in elastic adhesive films at the critical separation distance from ~3 at higher thicknesses to higher values at lower thicknesses. The transition occurs faster at higher thicknesses for films with a lower shear modulus.

wavelength is ~3h. However, for thinner films, the contribution for the surface tension force increases the wavelength to the longer-wavelength regime. The transition of the scaling factor for λ/h from ~3 to a higher value in the critical region is shown in Figure 6 for different values of the thickness and shear modulus. The graph shows that the transition occurs faster to higher values of the scaling factor for softer films with a lower shear modulus at higher thickness. Thus, when the surface tension parameter $\gamma/\mu h$ has considerable influence, it is possible to have a higher scaling factor for λ/h and thus a shift in the wavelength from short-wave to long-wave occurs even for purely elastic adhesive films.[41,48] This result is further verified through direct simulations shown later in the article.

As already discussed, in the case of an adhesive film, the destabilizing intermolecular interaction is a function of the contactor−film separation distance, and for a soft elastic film (low shear modulus), instability is possible for all reasonable film thicknesses.[47] However, for a wetting film, the strength of the intermolecular force is a function of the film thickness, and instability is possible only below a critical thickness (h_c). Figure 7 is an illustration of these critical thicknesses of wetting films for varying amounts of elasticity and surface tension for the films subjected to

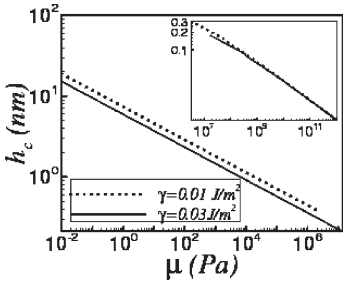

Figure 7. Critical thicknesses of films for varying amounts of elasticity (μ) and surface tension (γ). The plots represent values of $\gamma/\mu h$ higher than 1, and the inset represents values of $\gamma/\mu h < 1$. For thin films with greater than 1 nm thickness, the surface tension effects play an important role such that the inception of instability occurs only through long waves.

intermolecular interactions. The Figure shows that h_c decreases with increasing shear modulus (μ) and surface tension (γ) of the film. The Figure and its inset show that short waves, which require a small nondimensional parameter, $\gamma/\mu h < 1$, are possible only if the film thickness is in the subnanometer range, unless the film material is very soft ($\mu < 100$ Pa). Thus, for an unstable, soft thin viscoelastic wetting film, the surface tension always plays an important role and the instability is thus always long-wave, irrespective of whether the film has purely viscous or elastic or mixed characteristics.

It may be noted that unlike the dominant wavelength that is independent of rheology (discussed later in the section), the critical conditions ($\eta\omega_c/\mu$, $-hY_c/\mu$) and critical wavelength are strong functions of the elasticity of the film (μ). Strikingly, the critical conditions are also independent of the viscosity (η) of the film. Interestingly, Figure 7 shows that even the introduction of negligible elasticity, $\mu = 10^{-2}$ Pa, decreases the critical thickness to ~20 nm ($\gamma = 10$ mJ/m^2), which is otherwise infinite for a truly viscous film where $\mu \rightarrow 0$.[22]

Figure 8A shows the functional dependence of the dominant wavenumber (hk_m) and the interaction stiffness ($-hY/\mu$) of the film for different values of $\gamma/\mu h$. It is evident that hk_m increases (dominant wavelength decreases) with the increase in the interaction stiffness and decreases (dominant wavelength increases) with increasing effects of surface tension. Figure 8B show the variation of hk_m with $-h^2Y/\gamma$ [$= (-hY/\mu)/(\gamma/\mu h)$]. Dimensionless parameter $-h^2Y_c/\gamma$ is the ratio of the destabilizing intermolecular force to the stabilizing surface tension force. It is also evident from Figure 8B that under critical conditions the dominant wavelength is found to coincide with the critical wavelength and at values of interaction stiffness > critical the dominant wavelength is found to form the locus of the critical wavelength. The Figure clearly illustrates that there exist two distinct limits of the dominant wavenumber. As $-h^2Y/\gamma \rightarrow \infty$, the dominant wavenumber reaches a constant value of 2.12, independent of parameter $-h^2Y/\gamma$. This essentially results in the independence of the dominant wavelength ($\lambda \approx 3h$) with respect to the precise nature and magnitude of the destabilizing interactions. In this limit, the dominant wavelength is short-wave and is proportional to the thickness of the film. However, in the other limit where $-h^2Y/\gamma$ approaches 0, the dominant wavenumber is an increasing function of $-h^2Y/\gamma$ and thus the wavelength is highly dependent on the nature and magnitude of the interactions, as observed in experiments involving viscous films. The dominant wavelength in this limit is $2\pi/(-Y/2\gamma)^{0.5}$, which is equivalent to the wavelength obtained under the long-wave approximations that are valid for purely viscous liquid films.[3−14,16−34] This long-wave approximation

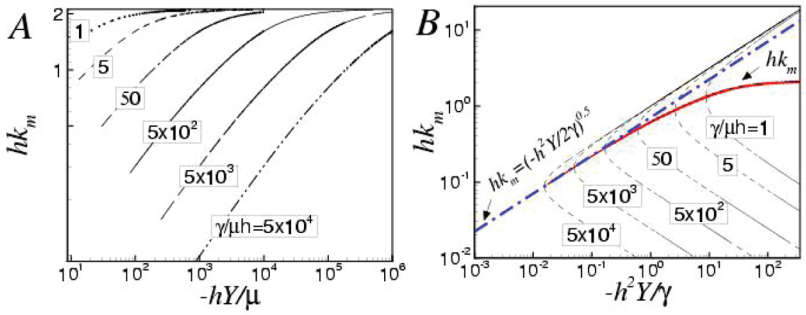

Figure 8. (A) Variation of the dominant wavenumber with the interaction stiffness for different values of the surface tension parameter, $\gamma/\mu h$. (B) The dominant wavelength is a function of $-h^2Y/\gamma$ only, independent of rheological properties μ and η. Dominant wavenumber hk_m forms the locus of hk_c. For lower values of $\gamma/\mu h$, $-h^2Y/\gamma$ tends towards infinity and the dominant wavenumber hk_m takes a constant value of 2.12, the limit for elastic adhesive films with short-wave instability. The dominant wavenumber merges with the long-wave approximation for $\gamma/\mu h \geq 5 \times 10^2$.

can also be obtained analytically with the help of the simplified dispersion relation obtained in eq 17. If the limit $kh \rightarrow 0$ is taken in the expansion of $S(kh)$ and terms up to fourth order (higher order terms being negligible) are kept in the expansion of $\exp[\beta]$, ($\beta = 2kh$ or $4kh$), then eq 17 simplifies to $\omega = h^3/3\eta[-Yk^2 - \gamma k^4]$, which on differentiation with the wavenumber yields the criteria for the dominant wavelength to be $2\pi/(-Y/2\gamma)^{0.5}$. Furthermore, if we consider the case of a wetting film destabilized by the van der Waals force ($-Y = A/2\pi h^4$), then it is evident that the dominant wavelength (λ_m) varies as h^2 (not linearly as in the limit of an elastic film). The crossover of the dominant wavenumber to the long wave occurs around $\gamma/\mu h \approx 5 \times 10^2$. Figure 8B also reveals that the dominant wavenumber depends only on the parameter $-h^2Y/\gamma$, making it independent of the rheological properties (μ and η) associated with the film in both the viscous and elastic limits. This is strikingly different from the strong dependence of the critical conditions and the critical wavelength in the viscoelastic films on the elasticity of the film. The above argument can also be proven analytically wherein it can be illustrated from the dispersion relation that to obtain the condition of dominant wavelength the following equation has to be satisfied: $(-hY/\mu)[S(q_m) + q_m S'(q_m)] + (\gamma/\mu h)q_m{}^2[S(q_m) - q_m S'(q_m)] = 0$. Thus, parameters $-hY/\mu$ and $\gamma/\mu h$ can be easily combined into a new parameter $-h^2Y/\gamma$, and the dominant wavenumber q_m is dependent only on this new parameter, which is devoid of any rheological quantity.

Figure 9 depicts the nondimensional characteristic time ($T\mu/\eta$ where $T = 1/\omega$) for the dynamics of instability. It is evident that as the value of $-h^2Y/\gamma$ increases, $T\mu/\eta$ decreases. This implies that the time required for the formation of patterns in a viscoelastic film is considerably lower than that for viscous films and in the limit of truly elastic materials the structures will develop instantaneously. Of course, this fast elastic timescale has to be tempered by the inertial effects. The Figure also shows that with an increase in nondimensional parameter $\gamma/\mu h$ the nondimensional time ($T\mu/\eta$) decreases for viscous films. However, the absolute time is higher for such viscous films as argued above because the nondimensional time has a factor of η/μ, which for viscous films has a large numerical value.

Equilibrium Morphologies of Adhesive and Dewetting Elastic Films. Morphological reorganization and pattern formation by the van der Waals force in thin, dewetting viscous films[1−23,25−28] and thin viscous films in adhesive contact[24] have been extensively studied. More recently, the patterns formed in elastic confined or adhesive films with van der Waals and electric fields have also been investigated.[37−39,43,45−56] A similar procedure of energy minimization is adopted in the present study to reveal the

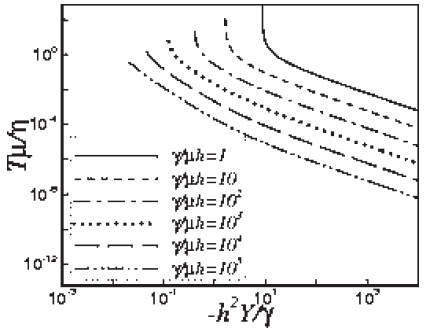

Figure 9. Nondimensional time required ($T\mu/\eta$) to form equilibrium structures as a function of $-h^2Y/\gamma$. The time required for viscoelastic films with higher elastic effects (with higher values of $-h^2Y/\gamma$) is considerably lower than that required for viscoelastic films with higher viscous effects (with lower values of $-h^2Y/\gamma$).

3D equilibrium morphologies of perfectly elastic adhesive and dewetting films with effects of surface tension and elastic stabilization included. The displacement (shape) of the film may be represented by its Fourier series constructed by the displacements in the direction normal to the free surface[46−48,53−56]

$$v(x,0,z) = \sum_{m=0}^{2M-1}\sum_{n=0}^{2N-1} v_{cc}(m,n)\cos(k_m x)\cos(k_n z) + v_{cs}(m,n)\cos(k_m x)\sin(k_n z) + v_{sc}(m,n)\sin(k_m x)\cos(k_n z) + v_{ss}(m,n)\sin(k_m x)\sin(k_n z) \quad (21)$$

where v_{cc}, v_{cs}, v_{sc}, v_{ss} are the Fourier coefficients and $k_l = (k_m{}^2 + k_n{}^2)^{1/2}$ is the wavenumber corresponding to m and n modes of deformation with $k_m = \pi m/L_1$ and $k_n = \pi n/L_3$. $2L_1$ and $2L_3$ are the length of the film along the x and z directions.

The total energy of the film is composed of the elastic strain energy $\Pi_E = \int_V \frac{1}{2}\sigma_{ij}\varepsilon_{ij}\,dV$ where σ is the stress tensor as defined in eq 3 neglecting the viscous part and ε is the strain tensor defined as the symmetric part of $\Delta\mathbf{u}$. The interaction energy is $\prod_U$, which is composed of the van der Waals attraction and a short-ranged Born repulsion, $\Pi_U = (-A/12\pi\xi^2) + (B/\xi^8)$. Here, ξ is the effective distance as discussed earlier, defined differently for the two cases of adhesive and wetting films, A is the Hamaker constant ($\sim 10^{-20}$J), B is the coefficient of the Born repulsion set from the conditions at equilibrium distance d_e, $\prod'_U(d_e) = 0$ and $\prod_U(d_e)$ represent the adhesive energy, which is $\sim$10.6 mJ/m^2. The surface energy is given by $\Pi_S = \gamma\int_S \sqrt{1 + \left(\frac{\partial v}{\partial x}\right)^2 + \left(\frac{\partial v}{\partial z}\right)^2}\,dS$. Individual terms $\prod_E$, $\prod_U$, and

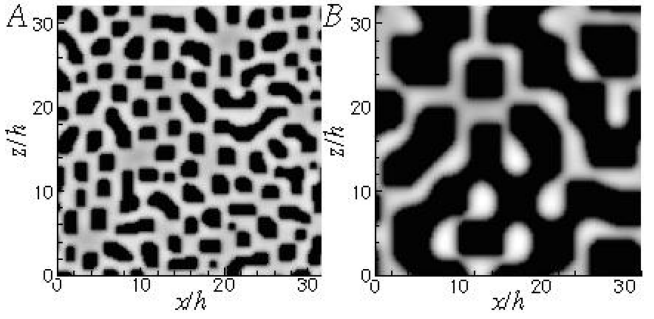

Figure 10. Labyrinth types of pattern formation at the surfaces of elastic adhesive films in contact proximity. The darker regions are the regions of contact. Film parameters are $h = 0.1\ \mu$m, $\mu = 0.1$ MPa, $A = 10^{-20}$ J, and $\gamma = 30$ mJ/m^2 for A and $h = 10\ \mu$m, $\mu = 1$ MPa, $A = 10^{-20}$ J, and $\gamma = 30$ mJ/m^2 for B. For the former case ($\gamma/\mu h = 0.03$ ($\ll$1)), the dominant/critical wavelength is short-wave with $\lambda = 2.97h$ (2.96h predicted by theory), and for the later case ($\gamma/\mu h = 3$ ($>$1)), the dominant/critical wavelength is long-wave with $\lambda = 6.4h$ (6.14h predicted by theory).

$\prod_S$ can be expressed in terms of Fourier coefficients v_{cc}, v_{cs}, v_{sc}, and v_{ss}, and thus the total energy of the elastic film becomes a function of these coefficients. For a given thickness of the elastic film, the equilibrium profile of the film surface (eq 21) is obtained by minimizing the total energy ($\prod_E + \prod_U + \prod_S$) in terms of these Fourier coefficients using a conjugate gradient minimization algorithm. The Fourier coefficients in eq 21 are initially assigned small random values to initiate the search process for obtaining the minimum-energy configuration. The energy-minimized configurations that evolve are stable against small random perturbations. Further details of the method and a discussion of locally metatable states in elastic films can be found elsewhere.[45−49,53,56] The minimum-energy states (shapes) are the equilibrium surface profiles that do not undergo any further coarsening. In fact, there is no mechanism of coarsening such as flow or diffusion present in an elastic film.

Figure 10 reveals the surface morphologies of elastic adhesive films in contact with a rigid contacting surface separated by the critical mean distance at which the instability is initiated. Figure 10A depicts the case of a film with thickness $h = 10\ \mu$m, $\mu = 1$ MPa, and $\gamma = 30$ mJ/m^2, and Figure 10B shows a film with the same surface tension value of 30 mJ/m^2, thickness of 0.1 μm, and shear modulus of 0.1 MPa. Both interfaces show a labyrinth type of pattern where the darker regions are the regions in contact and the lighter regions are the out-of-contact depressions formed on the film surface. Both Figures have an area of $32h \times 32h$. The difference in the two Figures, however, lies in the wavelength of the patterns formed. The former case exemplifies a short-wave elastic instability with a length scale of $\lambda = 2.97h$ as obtained through simulations, which compares favorably to the value of $\lambda = 2.96h$ predicted from the linear theory (Figure 5). The latter simulations represent a longer-wave instability with $\lambda = 6.4h$, which is also in agreement with the linear theory predictions of 6.14h. These results are also expected because for the first case the value of parameter $\gamma/\mu h$ is 0.03 ($\ll$1), which is within the limit of short-wave instability. For the latter case, the crossover of λ/h to higher values occur as $\gamma/\mu h = 3$ ($>$1) in this case. These simulations further confirm that for elastic adhesive films the instability length scale is indeed tuned by parameter $\gamma/\mu h$.[41,48] It may be noted that for adhesive elastic films with short waves (for example, the simulations in Figure 10A) the areas of contact with the external contactor are flat and the intersurface distance from the edges increases rapidly so that the VDW interaction outside of contact has a negligible contribution. This point is well known from the previous publications cited on purely elastic films. Thus, a simplified van der Waals potential used here by neglecting the curvature effect is suitable for illustrating the instability.

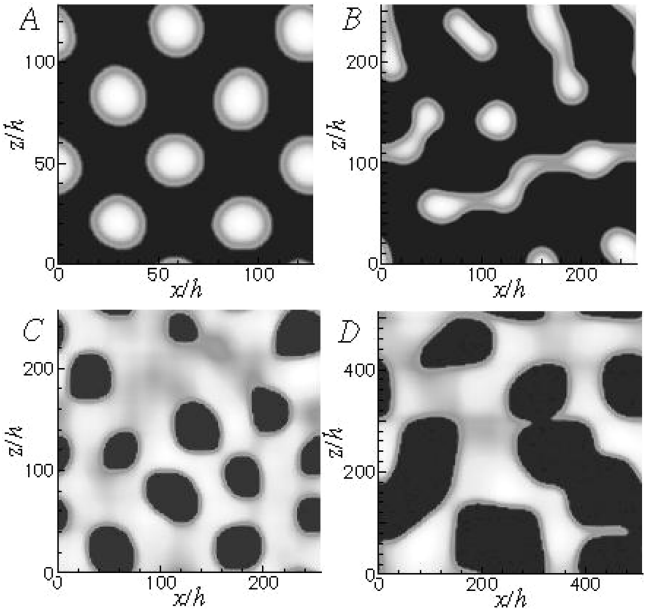

Figure 11. Morphologies of wetting films at critical thicknesses for (A) a film with a thickness (h_c) of 2 nm and a surface tension (γ) of 10 mJ/m^2; (B) a film with $h_c = 2$ nm and $\gamma = 30$ mJ/m^2; (C) a film with $h_c = 3$ nm and $\gamma = 10$ mJ/m^2; and (D) a film with $h_c = 5$ nm and $\gamma = 30$ mJ/m^2. The wavelengths obtained from simulations and predicted by theory for the films are (A) 90.5 nm (from simulations) and 90.5 nm (from theory), (B) 162 nm (from simulations) and 155 nm (from theory), (C) 213 nm (from simulations) and 202 nm (from theory), and (D) 905 nm (from simulations) and 997 nm (from theory).

Figure 11 shows equilibrium morphologies of elastic wetting films at their critical thicknesses. Figure 11A,C represents films with a surface tension value of 10 mJ/m^2 and critical thicknesses of 2 and 3 nm, respectively, and Figure 11B,D represents films with a surface tension value of 30 mJ/m^2 and critical thicknesses of 2 and 5 nm, respectively. The corresponding shear moduli for these films (Figures 11A−D) are obtained from Figure 7 and have values of 613.2, 215, 83.4, and 2.4 Pa, respectively. For the soft elastic films (Figures 11 A−D), the dominant wavelengths are obtained from the Fourier analysis of the equilibrium morphologies and have of values 90.5, 162, 213, and 905 nm, respectively. The linear stability analysis based on the van der Waals force predicts the critical/dominant wavelengths to be 90.5, 155, 202, and 997 nm, respectively. Thus, it is evident that the two results are in good quantitative agreement. The wavelength increases with the thickness of the film. In fact, it has the same scaling as for a wetting viscous film, namely, the dominant wavelength in this case increases as $\sim h^2$. This shows that irrespective of the film rheology the instability in wetting films always has long-wave character in both viscous and elastic films and also in general viscoelastic films. This is in contrast to a relatively thick elastic adhesive film where the short wavelength increases linearly with the film thickness. The long-wave nature of viscoelastic wetting films is understood by noting that the critical thicknesses of these films are very small and the values of parameter $\gamma/\mu h$ for these films are thus very high. From Figure 8, it is evident that in this regime (where $\gamma/\mu h \approx 10^3-10^6$) the critical or the dominant wavelength is dependent on the interaction stiffness and for VDW

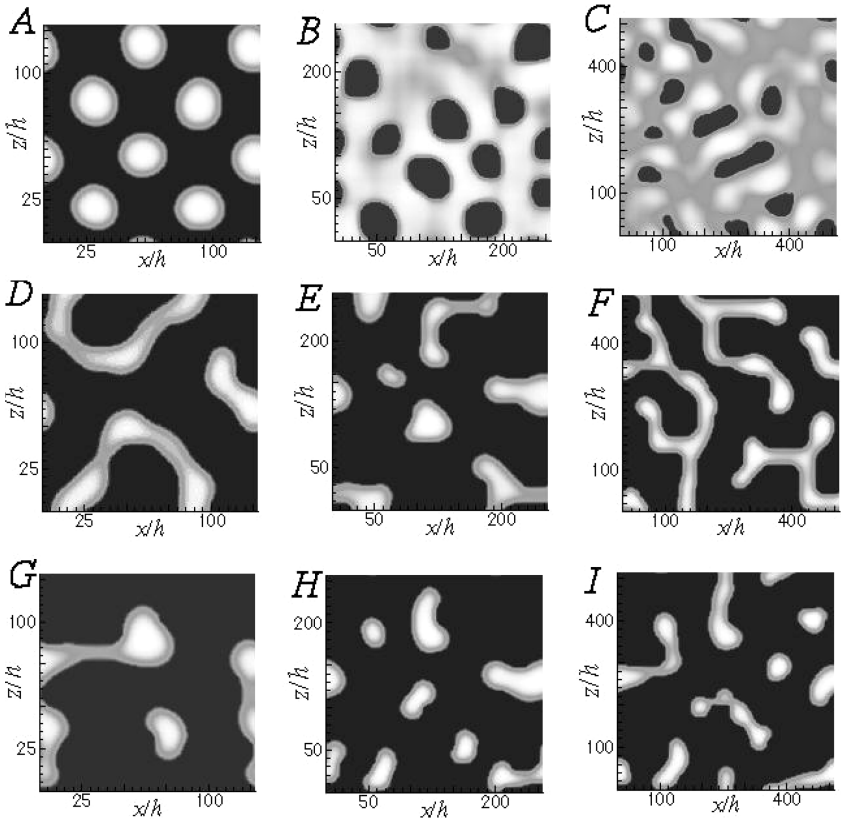

Figure 12. (A−C) Films with a surface tension of 10 mJ/m^2 and critical thicknesses of 2, 3, and 5 nm, respectively. The dominant wavelengths obtained from simulations are 90.5, 213, and 572 nm, respectively, compared to theoretical values of 90.5, 202, and 555 nm, respectively. Below their critical thicknesses, the film surfaces take the form of an interconnected chain of islands of higher thickness surrounded by a film of equilibrium thickness. For other physical conditions that are the same as in panel A, films below their critical thicknesses in panels D and G have thicknesses of 1.8 and 1 nm, respectively. The primary and secondary wavelengths of these films are 103 and 73 nm in panel D and 57.2 and 25 nm in panel G, respectively, and the neutral wavenumbers are 126 and 69 nm in panel D and 157 and 16.5 nm in panel G, respectively. Below the critical thicknesses for other physical conditions that are the same as in panel B, films in panels E and H have thicknesses of 2 and 1.5 nm, respectively. The primary and secondary wavelengths of these films are 229 and 110 nm in panel E and 135.8 and 60 nm in panel H, respectively, and the neutral wavenumbers are 314 and 74 nm in panel E and 314 and 36.5 nm in panel H, respectively. Below the critical thicknesses for other physical conditions that are the same as in panel C, films in panels F and I have thicknesses of 4.5 and 3 nm, respectively. The primary and secondary wavelengths of these films are 639 and 515 nm in panel F and 362 and 210 nm in panel I, respectively, and the neutral wavenumbers are 707 and 428.4 nm in panel F and 942.5 and 157 nm in panel I, respectively.

interactions give $\lambda \approx h^2$. The morphologies from simulations also reveal a striking feature that the linear stability analysis fails to provide. The morphologies show that irrespective of the effect of surface tension, when the critical thicknesses of the films are small, the structures formed are islands surrounded by air. In the Figure, the darker regions of the contour plots denote regions of smaller thickness and the lighter regions are regions of higher thickness. At higher critical thicknesses, the equilibrium morphologies obtained are opposite of those obtained for lower thickness. The instability now produces equilibrium structures of holes embedded in the surroundings of higher thicknesses. These reverse morphological structures obtained in perfectly elastic wetting films are reminiscent of the same island and hole structures obtained for thinner and thicker viscous liquid wetting films, respectively,[2,5−7,9,13,14,16,21,22,24,28] upon dewetting.

Figure 12A−C show the equilibrium surface patterns for films at critical thickness. When the thickness of the film is less than the critical, the equilibrium film surface increasingly takes the form of a chain of connected islands, irrespective of the surface morphology (islands or holes) displayed for this system at the critical point. For a purely elastic film with no viscous component, there is no dominant wavelength but there are two critical wavenumbers in the unstable region as seen in Figure 2. Interestingly, the simulation of Figure 12 also fails to show a single dominant wavelength but displays instead two significant wavelengths, primary and secondary, where the intensity of the Fourier coefficients are highest and second highest. These wavelengths are in between the neutral/critical wavelengths as predicted from linear theory. In fact, the bimodality observed in simulations gives the two wavelengths that are close to the two neutral wavelengths predicted from linear theory when the film thickness is slightly below its critical value. Physically, this primary wavelength can be viewed as the interchain separation distance where as the secondary wavelength resembles the distance present between the individual intrachain islands. For the wetting films, both the primary and the secondary wavelengths decease to lower values as the film thickness decreases further from its critical value, indicating a stronger instability (as shown in the caption of Figure 12).

Conclusions

We have presented a unified theory of the stability of soft viscoelastic thin films that uncovers the conditions and different regimes of instability in systems of nanoscopic to microscopic thickness from purely viscous liquids to purely elastic solid materials, from short to long waves, and from wetting to confined film geometries. Furthermore, conclusions based on the linear stability analysis are both verified and extended by simulations for thin, soft elastic films. Although we have chosen the long-range

attractive van der Waals destabilizing force for the specific numerical results displayed here, the equations and methodology presented are general for any form of destabilizing potential, including the electric field.

The significant findings of the linear stability analysis and numerical simulations carried out in the present study are summarized below.

(i) A purely viscous film is unconditionally unstable even for a vanishingly small attractive force. However, the introduction of solid, zero-frequency elasticity introduces the concept of a finite critical force or critical thickness for the initiation of instability. Instability at the film surface is possible when the interaction stiffness of the destabilizing force exceeds a critical value determined by the elastic stiffness and surface tension. The bifurcation diagram shows that the instability zone is enclosed between two neutral wavenumbers (where the growth rate is zero). At the critical point, these two neutral wavenumbers merge into a single critical value marking the maximum growth rate. The instability zone shrinks in area with increase elasticity and surface tension effects because the introduction of both of these effects makes it difficult for the film to develop surface instabilities. This effect is captured in computations of the increased critical interaction stiffness ($-hY_c/\mu$, $-h^2Y_c/\gamma$), which is required to initiate instability with increased surface tension and shear modulus.

(ii) The critical wavenumber of viscoelastic films, both in wetting and adhesive configurations, has two asymptotic limits of short waves and long waves that are determined only by parameter $\gamma/\mu h$. The first limit is encountered if $\gamma/\mu h < 10^{-2}$. In this limit, the critical wavelength remains constant at 2.12 ($\lambda = 2.96h$), which is independent of rheology, the destabilizing force, and the surface energy! This was reported for relatively thick, micrometer thickness elastic films interacting with rigid contactors.[40−42,45−47,51,53−56] In the other limit where $\gamma/\mu h > 1$, the critical wavelength approaches the long-wave regime as commonly seen in viscous wetting films.[1−23,25−28] For a wetting viscoelastic film with physically realistic parameters (for critical thicknesses greater than 1 nm), the instability is always found to be long-wave. Thus, an experimentally observable transition between short and long waves by varying the elastic modulus, thickness, and surface energy is possible only in elastic adhesive films[41,48] where the scaling for λ/h changes from its purely elastic thick film value of ∼3 to much higher coefficients that depend on the parameter, $\gamma/\mu h$.

(iii) Critical conditions $\eta\omega/\mu > 0$ and $-hY_c/\mu$ required to initiate the instability are strong functions of the elastic properties of the film. The dominant wavelength of the film, in contrast to the critical conditions, is independent of the rheological properties and is only a function of nondimensional parameter $-h^2Y/\gamma$.

(iv) As in the case of the critical wavelength, there are also two distinct limits for the dominant wavelength: the short-wave limit that is independent of the force and rheology ($hk_m = 2.12$) and the long-wave limit where the wavelength is nonlinearly dependent on the magnitude and nature of the destabilizing interactions, film thickness, and surface energy ($hk_m = (-h^2Y/2\gamma)^{0.5}$).

(v) As anticipated, linear stability analysis shows that the time of evolution of the patterns increases with viscosity and is thus negligible for purely elastic films when its fast dynamics (inertia) is neglected.

(vi) The simulation results show that these equilibrium morphologies for purely elastic wetting films (as also commonly observed in viscous wetting films) are all long-wave and have two distinct morphological signatures for higher and lower critical thicknesses. At lower critical thicknesses, the structures formed are islands surrounded by films of equilibrium thickness. For higher critical thicknesses, the structures formed are holes surrounded by the film phase. Finally, unstable wetting elastic films with thicknesses lower than the critical thickness are found to form interconnected islands with a bimodal distribution of wavelengths.

Acknowledgment. This work was supported by World Class University Grant No. R32-2008-000-20082-0 of the Ministry of Education, Science and Technology of Korea and by a DST IRHPA grant (India).